Selective Gate Driving in Intelligent Power Modules

Julio Brandelero, *Member, IEEE*, Jeffrey Ewanchuk, *Member, IEEE*, and Stefan Mollov, *Member, IEEE*

***Abstract*—Due to practical limitations in the manufacturing of power semiconductor dies, high power modules are composed of several dies in parallel in order to meet the desired load current requirements. With careful attention to the design, modern insulated gate bipolar transistor (IGBT)-based power modules feature relatively balanced current distribution amongst the parallel dies. However, owing to the increased switching speeds of wide bandgap devices, i.e., silicon carbide (SiC), it is challenging to design the package to achieve both low-loss and balanced operation. In this article, a technique is proposed where the individual dies in a multi-die power module can be selectively driven by a closely integrated gate buffer. Amongst the benefits achieved by selectively driving the die gates, a profiling of the power loss within the intelligent power module is enabled. Furthermore, a practical technique to estimate the individual die temperatures is presented, and using the same method, the on-state voltage of the power module during load current conduction can be estimated. Finally, it is experimentally demonstrated that the combination of individual junction temperature estimation and the selective gate driving can be used to increase the power density of the power module by better utilizing the component dies.**

***Index Terms*—Driver circuits, gate driver, multichip modules, power semiconductor devices, SiC devices, temperature balance, temperature control, temperature measurement, thermal balance, voltage measurement.**

I. Introduction

The rapid development of power electronics has enabled an increasing electrification of our every-day lives. However, further adoption of power electronics in harsh environments and critical applications, amongst which energy generation and distribution and aerospace, require a significant increase in their reliability in order to be considered for their large-scale adoption [1]. Thus, a significant amount of research effort has been dedicated to understanding how to improve the availability of power electronic converters, for example with the highly efficient and reliable smart transformer project for distribution systems [2], or the reliable power electronics project for high voltage transmission systems [3].

On another axis, wide bandgap power semiconductors, such as silicon carbide (SiC) or GaN are maturing and have an important role in improving the power density of power electronic converters. Due to the high dv/dt and di/dt from these power devices, and particularly related to the electrical parasitic elements from the power device packaging, the gate driver design is critical to exploiting the maximum performance [4]. One emerging trend, especially relevant for GaN power devices, is to integrate the gate driver close to the power semiconductor switch, i.e., as shown by GaN Systems [5], and Navitas Semiconductor [6]. Moreover, the limitation on the current capabilities of the devices lead to chip parallelization, as shown in Fig. 1, with advanced packaging structures and symmetrical layouts in order to achieve high power [7]–[9]. An intelligent power module approach with parallel dies that incorporates gate buffers tightly coupled to each individual die is presented in this article. This allows for a reduction in the switching losses by reducing the total gate loop inductance, minimizes the interaction with the load current through the emitter/source inductance during the switching and helps to distribute the current during the transition time [5], [6], [10]–[11].

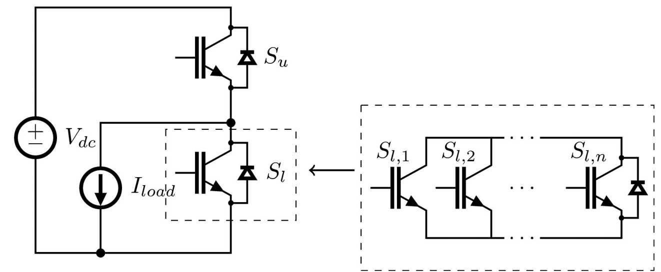

Fig. 1. Half bridge topology in a power module with *N* dies per switch.

Active gate driving concepts with more intelligence integrated in the gate driver are proposed to overcome some limitations from the power device packaging, as shown recently with a multilevel active gate driver [12], and active gate drivers with controlled output voltages [13]–[15]. A further development in integrated gate drivers is the inclusion of condition monitoring technologies to reduce the lifecycle cost of the converter with just-in-time maintenance [16]–[21]. In particular, these gate drivers incorporate on-board analog-to-digital converters (ADC), and computational intelligence to estimate the approximate state of health of the converter, i.e., by measuring the on-state voltage [17], estimating the junction temperature [19] or by estimating the thermal resistance [20], [21]. A technique using only the gate terminals that allows for the estimation of the individual junction temperatures of each die is presented in this article. The technique is then extended to allow for measuring of the on-state voltage of the power module during operation [38], and thereby enabling certain condition monitoring functions.

Manuscript received February 3, 2020; revised April 26, 2020; accepted June 2, 2020. Date of publication June 11, 2020; date of current version September 4, 2020. Recommended for publication by Associate Editor A. Lindemann. *(Corresponding author: Julio Brandelero.)*

Julio Brandelero and Stefan Mollov are with Mitsubishi Electric Center Europe, 35708 Rennes, France (e-mail: j.brandelero@fr.merce.mee.com; s.mollov@fr.merce.mee.com).

Jeffrey Ewanchuk was with Mitsubishi Electric Center Europe, 35708 Rennes, France. He is now with Research Center, Raytheon Technologies, East Hartford, CT 06108 USA (e-mail: ewanchje@rtx.com).

Color versions of one or more of the figures in this article are available online at https://ieeexplore.ieee.org.

Digital Object Identifier 10.1109/TPEL.2020.3002188

While current balancing between power modules is extensively treated [7], [21]–[27], it is recognized [28] that the approach does not address the actual stressor—the dies' junction temperature. In addition, the implementation of inter-die static and dynamic current equalization is impractical, due to the extreme requirements on the current sensors: large bandwidth, noise immunity, harsh environment, complexity of integration, and lossless operation. In this article, we propose a method of selectively driving the gate of each die, that uses a closed-loop algorithm for steering the losses and thus equalize the die temperatures.

The rest of this article is organized as follows. Section I of this article discusses the benefits and the drawbacks when using smaller and numerous parallel dies. In Section II, the proposed approach to better utilize and monitor the paralleled dies in a power module thanks to the per-die driven gates. The junction temperature and the on-state voltage measurement techniques, enabled by this approach, are also presented in Section III. In Section IV, the techniques to redistribute the thermal stress amongst the parallel die. Finally, it is experimentally shown in a SiC MOSFET prototype and in a Si insulated gate bipolar transistor (IGBT) prototype that the power module can handle up to 25% more load current by internally balancing the die temperatures through the better utilization of the dies within the power module.

II. Multidie Limitations in High Current Power Modules

Multidie power modules are commonly used to commutate large currents. However, in terms of cost, it is not obvious why less numerous, larger dies might be preferred over smaller, more numerous dies. This section reviews the benefits and drawbacks of a multidie power modules.

A. Benefits of Using Smaller Dies

While the general trend of high power modules is to increase the individual die size, and therefore reduce the number of parallel dies in a power module, it is not a general rule that larger dies are better in operation than smaller, more numerous dies. In terms of cost and thermal spreading, smaller, more numerous dies have a distinct advantage over their larger equivalent dies.

As a motivating example, an arbitrary 6″ circular wafer is considered, where the composite dies on the wafer have a square shape with an increasing die width in mm. Given the shape of the wafer, and an assumed thickness of wafer saw, a number of dies can be obtained from the wafer, as shown in Fig. 2(a). As the die size increases, the number of dies obtained from a single wafer eventually decreases. However, with a standard defect density of 0.1 defects/cm^2, the total number of dies is dramatically reduced compared to that of the zero defect density case. Therefore, as the final cost of the semiconductor component is related to the yield, it is clear that smaller devices can result in lower manufacturing costs.

Furthermore, smaller dies can better utilize thermal spreading to achieve lower thermal gradients when compared to larger dies. As shown in Fig. 2(b), two synthetic designs of a power module

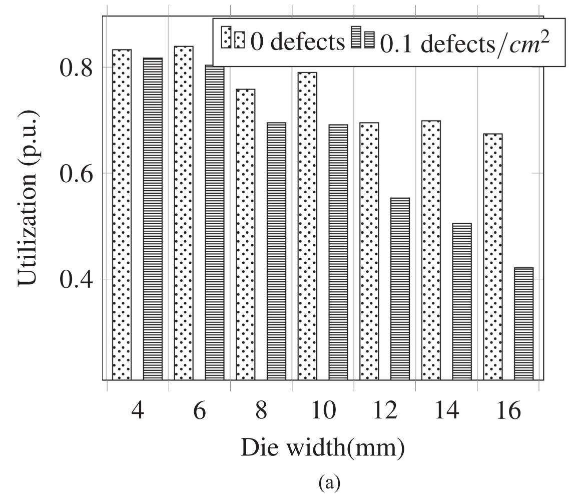

(a)

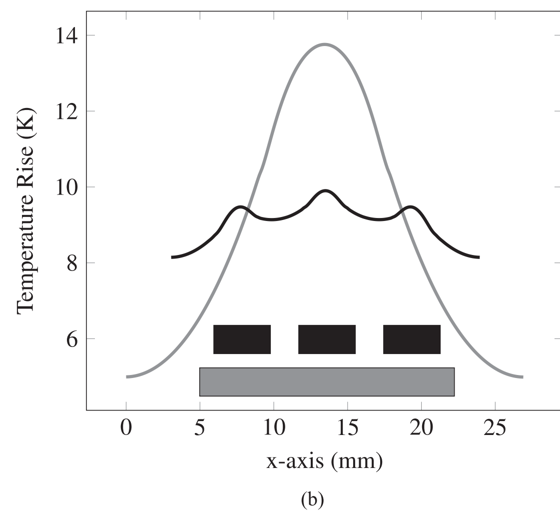

(b)

Fig. 2. Benefits using smaller dies (a) yield of a wafer as a function of die width (mm) for two defect densities, and (b) temperature rise across the linear distance of a single die (gray) against three dies with a similar total area (black).

with a traditional package were analyzed using a finite element method, assuming a fixed loss density of 20 W/cm^2.

The first design employs a single die to meet the design target, and exhibited a maximum thermal gradient of 14K across the surface of the die. Alternatively, a design assuming three parallel smaller dies (5 mm versus 16 mm) featured a maximum of 10K across each surface of the individual dies. While the average temperature of each solution was identical, the temperature distribution of the multidie solution was more even, and the peak temperatures were smaller. Therefore, smaller dies can simultaneously result in lower manufacturing costs, and lower temperature gradients on the surfaces of the individual components.

B. Drawbacks With Smaller and More Numerous Parallel Dies

Unfortunately, there are a number of drawbacks to using more numerous parallel dies to achieve a given load current rating in a power module. First, the design of the power module must accommodate the electrical and thermal connection to the external world to each individual component.

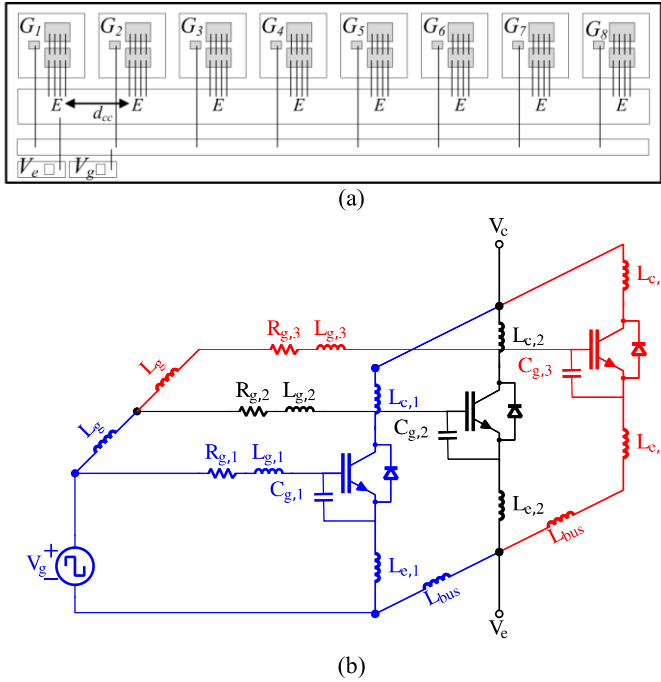

Fig. 3. Gate driving multidies module. (a) Substrate connection with a common emitter/source layout for eight parallel dies. (b) Electrical schematic of the parasitic network of three parallel dies in common emitter.

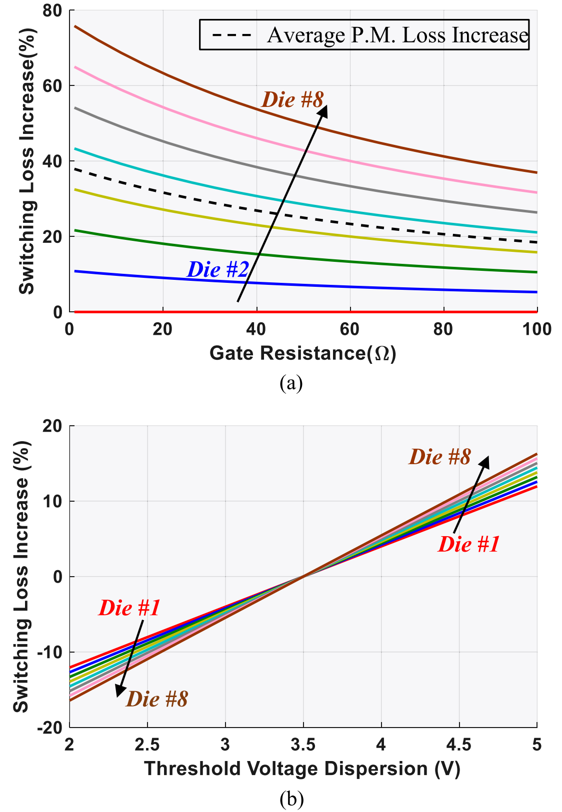

Fig. 4. Turn-ON switching losses across eight parallel dies. (a) With increasing gate resistance. (b) Increasing threshold voltage dispersion.

Owing to the differences in the power loop impedance and the driving loop impedance, the current distribution between the parallel devices is not ideal [22]–[24]. Layout techniques and guidelines to avoid derating on power modules concentrate the effort in reducing the parasitic impedances and having it symmetric [29]–[32]. Paralleling half-bridges instead of dies were shown [7], [34] to improve current sharing. While the current balancing issues can be reduced by using a common kelvin connection, the impact of a non-ideal electrical layout within the power module on the distribution of switching losses can be drastic [34]. Furthermore, as the thermal path cannot be guaranteed to be the same for all the dies, the temperature imbalance occurs even for a same power dissipation in each parallel die.

As a motivating example, eight parallel dies form an equivalent switch and are connected as shown in Fig. 3, with a spacing of $d_{cc} = 1.8$ cm, a bus-bar inductance of 5 nH/cm, and a bond wire inductance of 10 nH. The incremental source/emitter inductance in this example follows (1). In total, the source/emitter path difference differs by up to 9 nH, with a total source/emitter inductance of 19 nH from the distance of the gate pad to the last die in the parallel set. This total source/emitter inductance impacts the switching losses by modifying the applied gate voltage, $v_{ge}(t)$ as shown in (2), as detailed in [10] and based on the analytical work presented in [35]

$$\Delta L_s = n \cdot L_g \cdot d_{cc} \tag{1}$$

$$E_{\text{loss}} \propto L_s g_{fs} \exp\left(-\frac{t}{R_g C_{iss} + L_s g_{fs}}\right) \tag{2}$$

where g_{fs} is the transconductance of the MOSFET.

Given then a common emitter/source inductance design, the distribution of switching losses between the furthest MOSFET die to the nearest MOSFET die can be severe, though increasing the gate resistance can mitigate this unbalance to some extent, as shown in Fig. 4(a). The relative increase of switching losses from one die in Fig. 3(a) to the first die, with the smaller gate driver path, is considered with only the turn-ON transition and neglecting the reverse recovery of the inverse diode. In this case, a low gate resistance implies a relative average difference of nearly 1.4 times the first die along the substrate in Fig. 3(a).

While topological compromises between thermal and parasitic requirements can be found, the semiconductor device parameters that vary due to the manufacturing also impact this current unbalance [24], [34]. In particular, the threshold voltage of each power device can differ, causing asymmetric switching losses [34], as shown in Fig. 4(b). Using the same assumptions under the switching conditions as in Fig. 4(a), with 3.5 V as the reference threshold voltage, the impact of increasing the threshold voltage across the neighboring seven dies is shown in Fig. 4(b) for the substrate layout of Fig. 3(a). Thus in this example, a threshold voltage variation of 0.5V can impact the turn-ON switching losses by over 10% in the furthest die. Consequently, as the threshold voltage cannot be compensated by the design of the electrical routing of the power module, the parallel dies can be selected by matching their electrical characteristics [37]—a step which naturally comes associated with a cost.

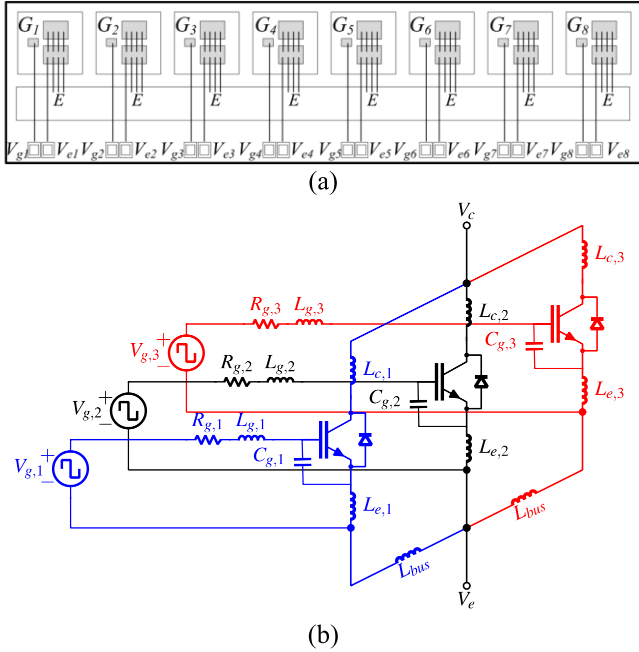

Fig. 5. Individual Gate drive of multidies module. (a) Layout of the substrate. (b) Individual gate driven equivalent electrical schematic.

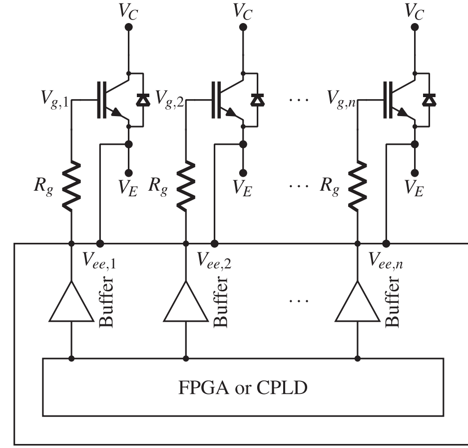

Fig. 6. Selective gate driven for intelligent power module: The integration of the individual gate buffers and coordinating control logic on the same emitter potential.

TABLE I
SWITCHING ENERGY VDC = 500 V, IDC = 40 A, PWM = 200 kHz, AND Rg = 12 Ω

Die	Single gate access		Selective gate driving	
Pos.	E_{on} (μJ)	E_{off} (μJ)	E_{on} &(μJ)	E_{off} (μJ)
1	142	3.54	113	5.80
8	195	7.64	89.2	12.4
5	-	-	139	9.67
avg	168.5	5.6	113.7	9.3

III. Selective Gate Driving of Power Modules

In this article, a solution to take advantage of the cost benefits of smaller, more numerous dies, while mitigating the adverse impact of the packaging and parameter mismatching is proposed, termed "selective gate driving," wherein each power die is individually driven. The substrate requires a modification in order to enable the individual access to each emitter/source pad, as shown in Fig. 5(a), similar to that required for Kelvin emitter/source access. Advantageously, the selective driving reduces the switching losses, increases the controllability and permits the per-die condition monitoring functions.

In this case, the parallel dies are on a common electrical reference and the addition of individual gate buffers, as shown in Fig. 6, does not require costly individual power supplies. This solution is designed to be compatible with the concept of intelligent power modules, where the gate driver and power dies are integrated within the power module structure. Another advantage of the selective gate driving is the increased controllability, whereby the dies can be delayed relative to each other, or enabled/disabled during a switching commutation. This allows the field programmable gate arrays (FPGA)/complex programmable logic device (CPLD) to manipulate the driving pattern to each die individually, without affecting the output voltage at the terminals of the power module—this will be discussed in Section IV

A. Reduced Switching Losses and Increased Controllability

The selective gate driving approach inherently shares a decoupled driving path from the neighboring dies, Fig. 5(b). Hence, it not only enables optimizing the power layout as proposed in [7] for improved commutation, but also allows for reduced switching losses of the dies impacted by the ΔL_s . This is attributed to the reduced interaction between parallel sets of power devices [10]. As a consequence, selective gate driving permits a power module loss saving by the amount indicated by the curve "average loss increase" in Fig. 4(a).

Taking for example the prototype of Fig. 15, the measured switching energies of SiC MOSFETs are given in Table I for the single gate access and with the selective gate driving approach. As expected from Fig. 4(a), the results show an average reduction of more than 30% on the turn-ON losses during the operation of the power converter.

B. Gate-Sensitive Parameters

This section presents two unique characteristics not otherwise possible without individual die control: individual junction temperature estimation (using the internal gate resistance) and on-state voltage estimation (using the input capacitance) without any power terminal connection. It is important to state that both methods of acquiring information relevant to the health state of the power module are performed during nominal operation and does not require interruption of the industrial process.

The gate path circuit is commonly modelled as a series resistance capacitance (RC) network for the metal oxide semiconductor (MOS) devices such as IGBTs and MOSFETs. The dependence of the internal gate resistance on the junction temperature is well known [37]–[41]. Coexistent with the gate resistance temperature dependence, the internal input gate capacitance, C_{ies} or C_{iss}, of the target semiconductor die is dependent on the drain-gate voltage and on the junction temperature above the

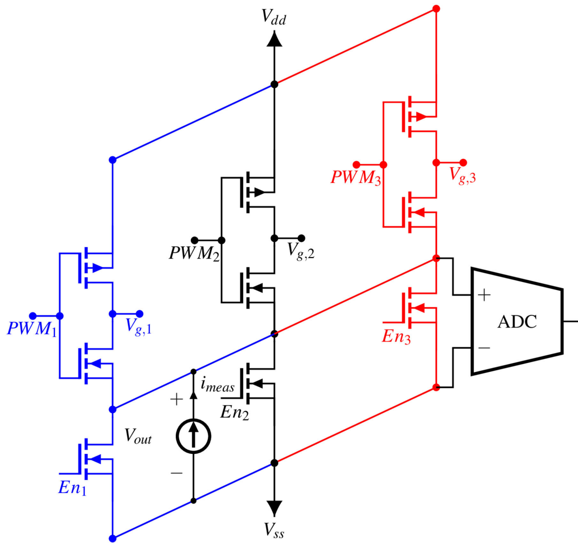

Fig. 7. DC gate injection circuit for a three die system with a measurement current i_{meas} and measured gate voltage corresponding to V_{out}.

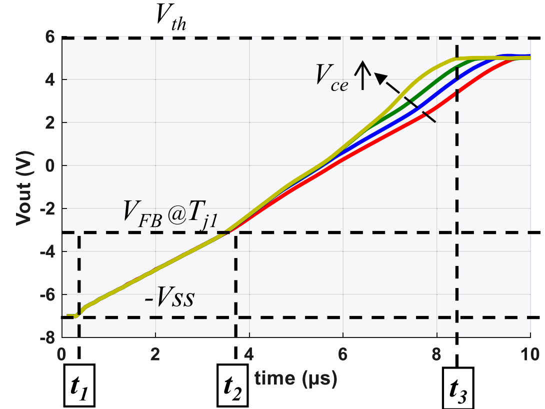

Fig. 8. Experimental waveform of the gate voltage of the inactive die with a constant injection current, and with various blocking voltages, from 0 to 3 V, across the inactive die at 25°C (IGBT ref: CM150TX).

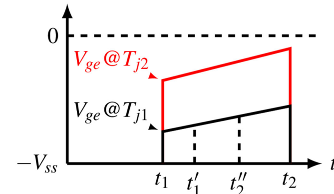

Fig. 9. Injection of the measurement current and corresponding gate voltage with two different values of the internal gate resistance due to two different temperatures, T_{j1} and T_{j2}.

flat-band voltage V_{FB} of the semiconductor device [42], in the depletion region.

Critically, in order to make the junction temperature measurement linearly dependent on the internal gate resistance alone, the measurement samples of the gate voltage must occur below the flat-band voltage, in the accumulation region. In this region, the gate-emitter capacitance is not dependent on temperature or frequency or collector-emitter voltage or the load current.

When the gate voltage is greater than the flat-band voltage V_{FB} of the MOS-gate semiconductor die, the internal gate capacitance C_{iss} of the target semiconductor die becomes dependent on the drain-gate voltage, as well as the internal junction temperature, described in [42] and [43].

One technique of measuring the internal gate resistance and the input gate capacitance by using one and the same circuitry is to inject a small reference current i_{meas} into the gate terminal of a specific die and then measure the related gate voltage V_{out}, as shown in Fig. 7 and described in [41].

Fig. 7 shows how multiplexing and control MOSFETs $En_{,n}$ are placed in between the negative power supply rail and the source of a standard totem pole gate buffer, from Fig. 6. In normal operation these control MOSFETs shunt the dc measurement current source i_{meas}, and make the source potential of the gate driver equal to the negative power supply reference V_{ss}. To perform the current injection, the target power die is turned-OFF, and when the respective control MOSFETs, En_j is opened, the measurement current flows into the gate of the target die.

The measured voltage V_{out} is an image of the gate voltage $V_{g,n}$, and evolves as in Fig. 8. The junction temperature can be determined by sampling the voltage across the control electrodes V_{out} between the time t_1 and t_2 where only the gate resistance is sensitive to the temperature. At t_2, the flat band voltage is reached. The voltage trajectories between t_2 and t_3 are then sensitive to the drain-source voltage and the temperature.

The normal switching pattern is not modified and the typical time to estimate T_j is a few microseconds. Note that only a single current source and ADC is necessary to estimate the T_j of each parallel die thanks to the multiplexer MOSFET *Enj*, reducing the associated cost. The optimized bill of materials of the associated electronics represents approximately 15% cost increase to popular industrial grade gate drivers available on the market.

C. Junction Temperature Sensing

Junction temperature estimation using thermally sensitive electrical parameters (TSEPs) in power electronics has seen an intensified interest as it is an essential indicator for the state of health of a power module [1]. However, to the best of the authors' knowledge, the TSEPs from literature cannot uniquely identify the individual die junction temperatures, T_{vj}, and the physical meaning of a single measurement for multi-die power modules indicates either an average or a singular/extreme die within the power module [38]. Therefore, a further advantage of having individual gate access to each die is the ability to interact with each die to perform individual junction temperature estimation. A number of TSEPs can be used with the gate circuit of a power device, and the temperature dependency of the internal gate resistance of the semiconductor device is particularly promising due to its customizable nature during die manufacturing [38]–[41]. Combining this TSEP with the selective gate driving concept then allows for the individual estimation of the junction temperatures of each die, as highlighted in [42].

As shown in Fig. 9, the simplest way to measure the temperature sensitive gate resistance is to sample V_{out} at time t_1.

At this instant, the measured voltage V_{out} is proportional to the injected current i_{meas} and the internal gate resistance of the die under measurement $R_{g,n}$ as per (3), but depends on the precision of the current source. In order to cancel the influence of the current source, a pair of samples is taken at instances t_1' and t_2''. In this period, the gate voltage evolves according to (4). By dividing the second measurement point by the difference between the first and second measurement as per (5), the value of the injected current is no longer present and the equivalent measurement is dependent on timing parameters, as per (6). During the calibration phase, all of the dies are heated at two distinct and known temperatures to determine the linear temperature variation of the gate resistance, i.e., *A* and *B* as per (7). The junction temperature of each die can be estimated during the operation of the power module using the individual current injection on each die according to the selective driving proposed in this article.

$$V_{\text{out}}(t_1) \approx V_{ge}(t_1) = R_g(T_j) \cdot I_{\text{meas}} \tag{3}$$

$$V_{ge}(t) = R_g(T_j)\, I_{\text{meas}} + t \cdot \frac{I_{\text{meas}}}{C_{ies}} \tag{4}$$

$$\text{TSEP} = \frac{V_{ge}(t_2'')}{V_{ge}(t_2'') - V_{ge}(t_1')} \tag{5}$$

$$\text{TSEP} = R_g(T_j) \cdot \frac{C_{ies}}{t_2'' - t_1'} + \frac{t_2''}{t_2'' - t_1'} \tag{6}$$

$$T_{j,est} = A \cdot \text{TSEP} + B \tag{7}$$

As the measurement occurs below the flat-band voltage of the semiconductor device, the gate-emitter capacitance is not dependent on temperature, and is also invariant to the collector-emitter voltage and load current. This result is confirmed in Fig. 10(a), where changing the bus voltage, the load current and the switching frequency show no impact on the temperature measurement, where TSEP is obtained as per (5), using the prototype described in Fig. 19.

Further confirming the performance on a six-die IGBT prototype, Fig. 10(b)–(c) shows two power modules using two different die references with integrated internal gate resistances of 13 and 2 Ω. respectively. In the former case, the precision is within 2K with a standard deviation of 0.66K. The latter case has precision of 5K, with a standard deviation of 2.4K. Hence, robust and individual junction temperature measurements are enabled with the selective driving technique.

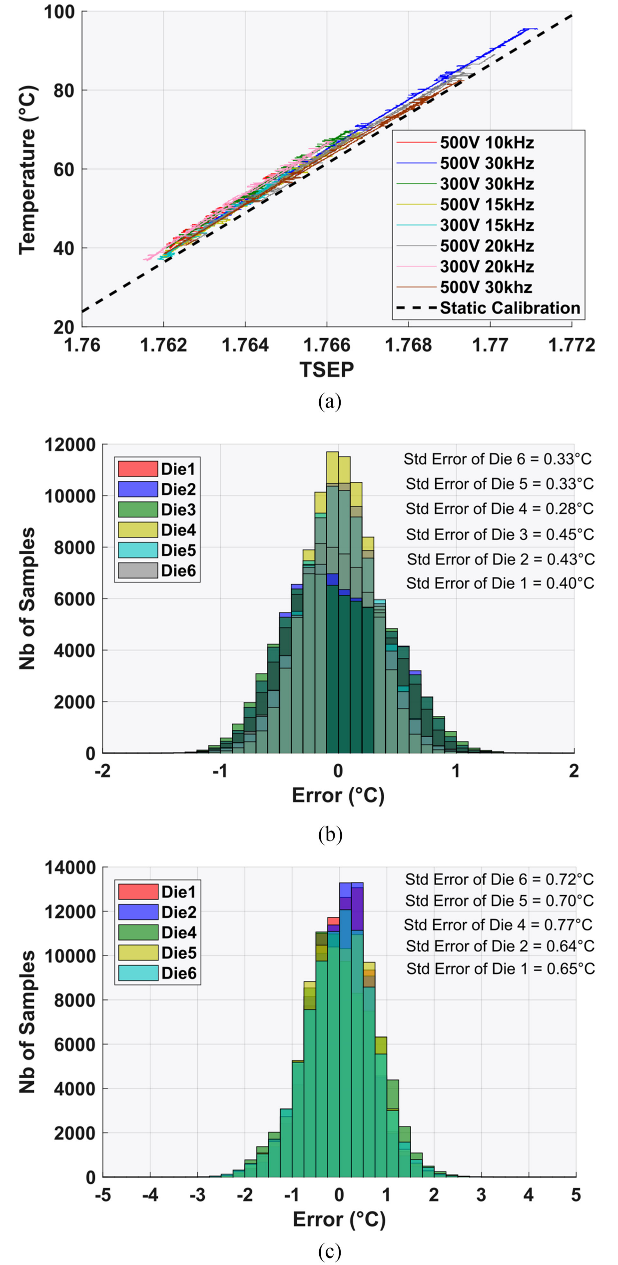

Fig. 10. Experimental junction temperature measurements from prototype of the Fig. 19. (a) TSEP as per (5) in function of the temperature variation on the gate of a single IGBT die (Rgint = 13 Ω) under changing dc bus voltage and switching frequency; temperature dispersion. (b) Power module with 13 Ω internal gate resistance. (c) Power module with 2Ω gate resistance.

D. Indirect On-State Voltage Measurements

Another advantage of selective gate driving is that the on-state voltage of the parallel set of dies can be indirectly measured using only the gate circuitry [43]. Consequently, high voltage devices that interface with the power terminals of the power module are not necessary, increasing the reliability of the gate driver.

In the method proposed in this article, the average on-state voltage of the conducting parallel dies is indirectly measured due to the inactive die blocking the on-state voltage, v_{on} of the parallel dies, as shown in Fig. 11.

Using the same dc measurement current injection circuit as per Fig. 7, the principal operation of the voltage measurement is enabled by increasing the current injection time to change the gate capacitance of the target semiconductor from a voltage-independent state to a voltage-dependent state (see Fig. 8). Therefore, one sample between instances t_2 and t_3 must be made to determine the on-state voltage. Consequently, relating V_{out} to v_{on} at a given temperature requires a two-dimensional calibration with linear approximation over small regions of V_{ce} as

$$v_{\text{on}}(T_j) \approx C\{T_j\}\, V_{\text{out}} + D\{T_j\}. \tag{8}$$

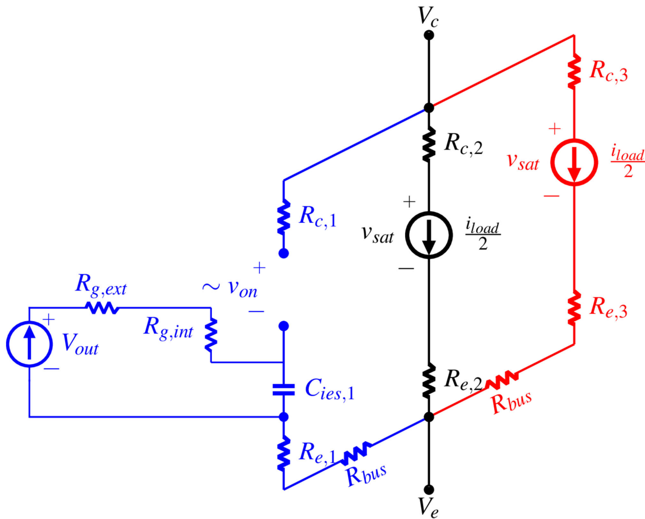

Fig. 11. On-state voltage measurement of the power module: equivalent electric circuit when one device is held off, while the neighboring devices are conducting current

The indirect saturation voltage measurement by selective gate driving is intended to perform condition monitoring on the interconnections of the power modules, i.e. to detect wire bond lift-OFF due to aging [1], represented by the resistance $R_{c\ 1,2,3}$ and $R_{e\ 1,2,3}$ on the Fig. 11. Therefore, the range of voltages to be measured is in the order of 0.5 to 3 V, depending on the power semiconductor under test.

Considering this test range, an experimental prototype was passively heated by a hot-plate, and a voltage was applied to the nonconducting device to mimic the reflected voltage of the neighboring dies when in operation.

In (8), each calibration coefficient $C\{T_j\}$ and $D\{T_j\}$ is derived from the calibration at a given junction temperature; more details on the relationship between the measured gate voltage and the corresponding saturation voltage can be found in [43].

The experimental results, from prototype of Fig. 19, for switching frequency of 20 kHz were plotted in Fig. 12(a) over the temperature range of 30°C to 100°C. We observe that above V_{CE} of 1.5 V, the relationship between V_{CE} and V_{GE} is linear and monotonic and it depends very weakly on the temperature, particularly in the higher temperature range.

Finally, after calibration of the circuit according to (7), Fig. 12(b) shows that a voltage measurement can be made with a precision of 20 mV, and a standard deviation of 6mV.

Assuming slowly-varying load current, the on-state voltage for each die can be obtained by sequentially applying the measurement sequence described earlier and solving a linear system of equation of order N (number of parallel dies). This enables another important means for condition monitoring of wire-bonded power modules.

IV. Equilibrating the Junction Temperatures

Within parallel-connected pulsewidth modulated (PWM) converters, adjusting the individual timing between these converters is used as a means of balancing the switching and conduction losses across the set of converters [25], [44]. Such systems require fast and accurate measurement for the control feedback [45], [46]. Individual timing calibration to match the switching current for paralleled devices is proposed in [26] using an automatic double pulse test bench within a production line. However, the motivation in this article is to correct the temperature imbalance, as shown in Fig. 13, within the power module instead, e.g., due to the thermal constraints caused by

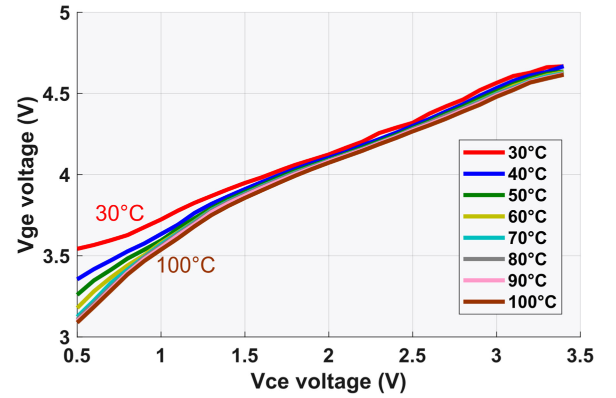

(a)

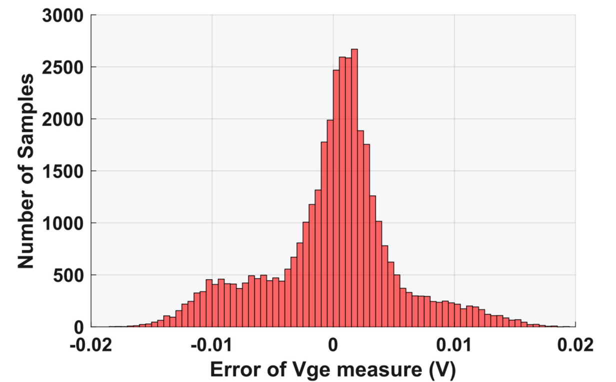

(b)

Fig. 12. Experimental on-state voltage measurements from prototype of the Fig. 19. (a) Increasing blocking voltage of an inactive die with changing gate voltage and temperature. (b) Distribution of the collector emitter voltage error samples using the described method with selective gate driving and the actual measurement.

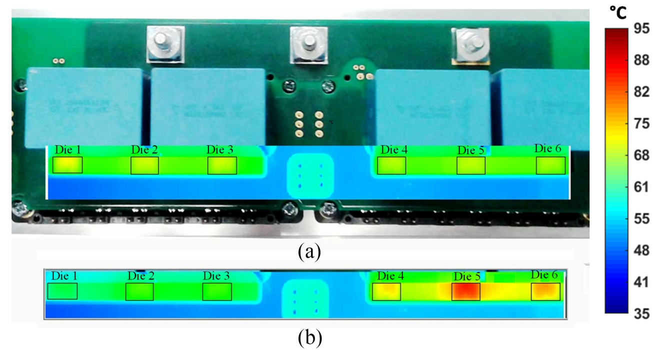

(a)

(b)

Fig. 13. Temperature distribution of the dies of the prototype of Fig. 18 at 78 A. (a) Thermo-controlled. (b) Classical gate driving.

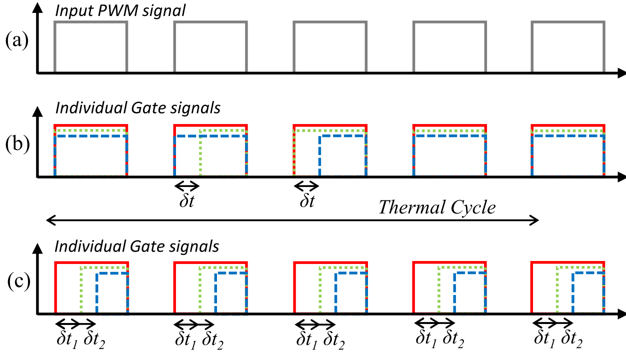

Fig. 14. Selective gate driving (a) Switch input PWM signal. (b) Individual gate signals for the fixed delay stress steering method. (c) Individual gate signals for the delay stress steering method.

the physical location of each die within the power module, and the electrical dispersion of the characteristics of the power dies, especially in the V_{th} of the SiC devices. This is based on the observation that most faults found in practice for power modules are intimately related to temperature. In this sense, the utilization of each die is improved by entirely removing the hot spots from the power module in operation, as it shown in Fig. 13. As the derating in multidie modules is motivated by the temperature of the hottest die, removing the hot spots by the application of the selective driving pattern effectively allows for an increase in the load current capability of the power module.

The target temperature $\overrightarrow{Tobj}$ of each die is defined as the average junction temperature, then a loss vector can be found in order to equalize the junction temperature as

$$\vec{P} = [R_{TH}]^{-1} \times \overrightarrow{Tobj}$$
$$\text{with } \vec{P} = [P_1, \ldots, P_N\ ]^T \text{ and } \overrightarrow{Tobj} = \left[\overline{T_j}, \ldots, \overline{T_j}\ \right]^T \quad (9)$$

where $[R_{TH}]$ is the thermal resistance matrix, of size *N*x*N*, with the self and coupled thermal resistances and $\vec{P}$ is the sought power dissipation vector of the *N* dies.

In order to manipulate the power losses and thus the temperature, a delay noted δt_n is applied at the rising edge of the PWM signal, thereby steering the losses in the remaining active dies. The incoming PWM signal is manipulated by the CPLD/FPGA controller (see Fig. 6) and the delay is applied selectively to the hottest dies. Two methods are proposed in this article.

First, a fixed delay δt can be used to completely eliminate the commutation and (partially) the conduction losses of the selected die during a switching period as it is shown in Fig. 14(b). The dies that tend to be hotter are delayed more frequently than the colder dies, as detailed in [47]. The delay is determined from a prior knowledge of the temperature distribution of the dies.

In a second solution, a variable delay δt_n is applied to each switching pulse, as in Fig. 14(c). The delay is determined through a closed-loop controller and evolves throughout the life of the power module in response to ageing.

Note that in both cases there is always at least one die commutating with the prescribed instants of the PWM pattern, thus the output PWM waveform on the switching node is not modified in the process.

A. Fixed Delay Stress Steering

The control duty cycle, d_j is introduced in (10) and refers to the ratio of the inactivity of the switch *j* per thermal cycle, as shown in Fig. 14(b). The thermal cycle incorporates a predefined number of sequential switching pulses. Furthermore, the depth of the thermal equalization intervention d_0 refers to the proportion of normal operation of the power module such that $d_0 = 1 - \sum_{j=1}^{N} d_j$, then the (11) is deduced from (10). For example, in Fig. 14, switches 2 and 3 are activated with a delay once within the thermal cycle out of four switching pulses, hence the duty cycle for the first die d_1 is zero and the duty cycles d_2 and d_3 are 25% for dies 2 and 3. The normal operation duty cycle d_0 is, therefore, 50%. In (13), the loss vector $\overrightarrow{P_0}$ contains the losses of the dies in normal operation and the vectors $\overrightarrow{P_1}$ to $\overrightarrow{P_N}$ contain the losses, $P_{i,j}$, of each die *j* when the respective die *i* is activated with the delay δt. Such partial die-shedding pattern is then applied cyclically and relies on the relatively large temperature time constant present in the structure of the power module.

For the purposes of temperature equalization, the duty cycle d_j, is calculated from (12), obtained from (9) and (11). As the duty cycles are limited in the range $0 < d_j < 1$, an optimization method may be applied to match the temperature requirement with a certain error due to the duty cycle constrains

$$\vec{P} = \left[\overrightarrow{P_0},\ \ \overrightarrow{P_1},\ \ldots\ ,\ \overrightarrow{P_N}\right] \times [d_0,\ d_1, \ldots,\ d_N\ ]^T$$
$$\text{with } \overrightarrow{P_i} = [P_{i,1}, \ldots, P_{i,j}, \ldots, P_{i,N}\ ]^T \quad (10)$$
$$\vec{P} = \left[\overrightarrow{P_1} - \overrightarrow{P_0}, \ldots,\ \overrightarrow{P_N} - \overrightarrow{P_0}\right] \times [\ d_1, \ldots,\ d_N\ ]^T + \overrightarrow{P_0} \quad (11)$$
$$[d_1\ \ldots\ d_N\ ]^T = \left([R_{TH}] \times \left(\left[\overrightarrow{P_1} - \overrightarrow{P_0}, \ldots,\ \overrightarrow{P_N} - \overrightarrow{P_0}\right]\right)\right)^{-1} \cdot \left(\overrightarrow{Tobj} - [R_{TH}] \times \overrightarrow{P_0}\right). \quad (12)$$

The concept described above was demonstrated using a SiC power converter with forced-air cooling to mimic the operation of the intelligent power module, see Fig. 15. Each power module is composed of eight parallel discrete devices (ref: C2M0160120D). The power impedance loop has been minimized using decoupling capacitors placed as close as possible of the switching cell to avoid overvoltage during the switching time and the individual gate buffers were similarly placed as close as possible to the power devices. The reference power module has the exact same bus bar layout, but a single gate driver for all the devices, with the gates and sources connected in parallel. The temperature has been measured using only an infrared camera.

The switching losses on the hottest and coldest dies were investigated experimentally on the reference power module and on the multigate access power module, as given in Table I. Using a fixed delay $\delta t = 20$ ns, the switching losses are measured for the switches 5 and 8 while the delay is applied on the switches 4, 5, and 8 on the multigate access power module and with the results given in Table II. The table also gives the ratio of

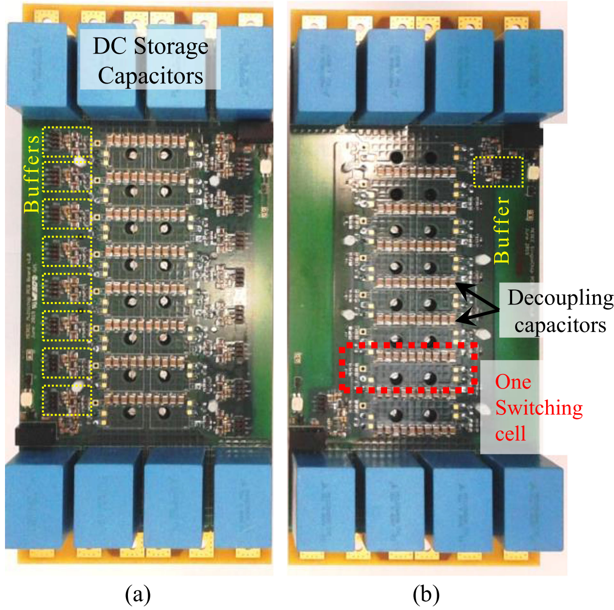

Fig. 15. Experimental prototype composed by eight paralleled SiC MOSFETs. (a) Selective gate driving module. (b) Classical driving module.

TABLE II
SWITCHING ENERGY OF SELECTIVE GATE DRIVING $\delta t_n = 20$ NS, VDC = 500 V, IDC = 40 A, AND PWM = 200 kHz

Die Pos.	D4 Delayed by δt_n		D5 Delayed by δt_n		D8 Delayed by δt_n	
	E_{on} (μJ)	Ratio	E_{on} (μJ)	Ratio	E_{on} (μJ)	Ratio
5	171	1.23	19.2	0.13	166	1.19
8	140	1.56	140	1.56	0.64	0.01

switching energy of the die in tests with delay compared to the measured switching energy without delay but with selective gate driving of Table I.

In Fig. 16, three temperature distributions on the experimental platform are illustrated: the reference case with a single gate driver for all eight parallel dies (SG)—the classical way the power modules are driven; the multigate driver for the eight dies with the multigate selective driving only (“MG w/o pattern”); and the same module with the application of stress steering with preset delay times (‘MG w/pattern). In the reference case, the hottest temperature is 82°C; note that the die at the position 1 is closest to the fan. The threshold voltage dispersion has a significant impact on the thermal distribution across the set of dies. In Fig. 16(b), the threshold voltages (Vth) are plotted with respect to the average Vth. High threshold voltage dies exhibit lower losses and lower junction temperature in the case without stress steering for the reference design with classical gate driving. This has been compensated for the module with temperature compensation (traces denoted “MG”) and die temperature is equalized despite wide threshold dispersion.

By simply applying the multi-gate access with individual gate buffers, the peak temperature decreases to 68°C [see Fig. 16(a), MG w/o pattern]. Note that for the same load conditions the average temperature is reduced, indicating also reduced total losses. This is attributed to more favorable commutation conditions, as indicated in Section III-A.

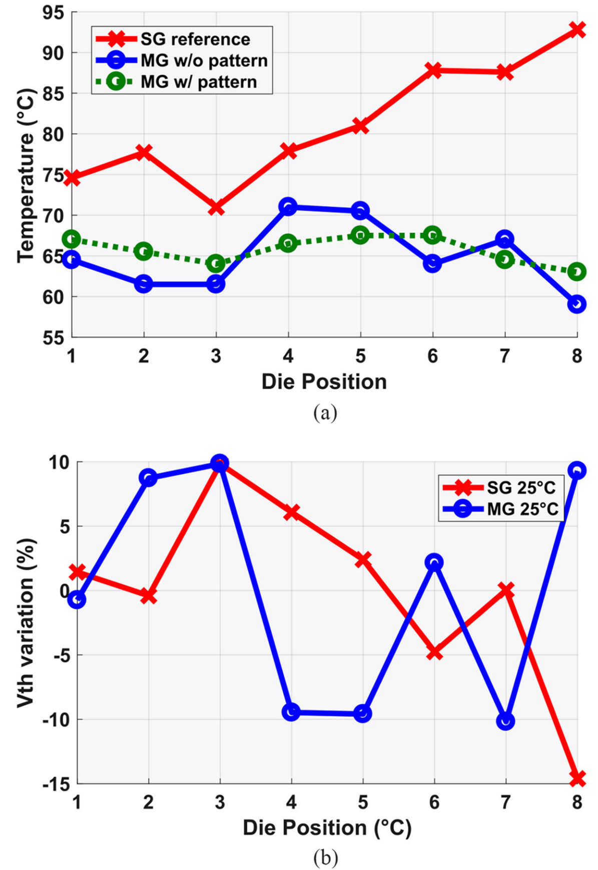

Fig. 16. Experimental data of the classical SG and the MG power modules. (a) Reduction of peak junction temperatures with and without fixed delay stress steering (w/o pattern). (b) Vth variation on the dies composing the modules.

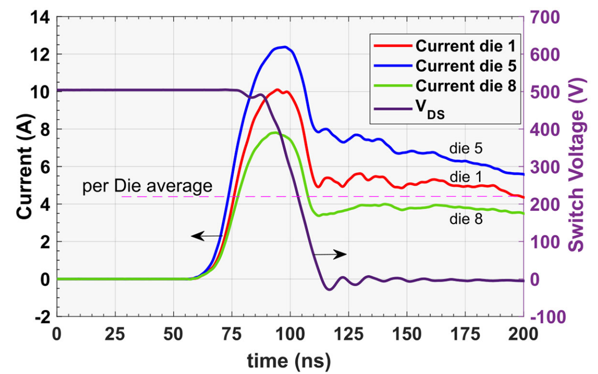

Fig. 17. Experimental waveforms of SiC prototype for a delay of $\delta t = [0, 2.2, 0.8]$ns for dies 1, 5 and 8 respectively.

Furthermore, by selectively driving the multi-die controller, using (12) [see Fig. 16(a), MG w/ pattern] with $[d_1, \ldots, d_N] = [0.047,\ 0,\ 0,\ 0.243,\ 0.215,\ 0,\ 0.194,\ 0]$, a further 5°C of peak temperature reduction is gained. This is achieved through redistribution of the internal power losses by accounting for device parameter and manufacturing spreads based on experimental measurement of the thermal resistance matrix$[R_{\mathrm{TH}}]$.

Fig. 17 captures the turn-ON transition of three out of eight parallel dies with the thermal equalization pattern applied.

The current is commutated within 50 ns, after which individual die currents slowly converge to the shared load current value—this is typically seen for parallel dies. We note that die 5 commutates first, despite the largest delay applied. Similarly, die 8 commutates last despite having applied delay smaller than die 5. It would, therefore, appear that the applied thermal equalization also contributes to current sharing for the cases where the losses are dominated by switching.

While the method described here is very effective in equating the junction temperatures at a low cost, it necessitates a relatively complex calibration procedure and, more importantly, does not respond to module evolutions such as deteriorating interfaces as ageing progresses

B. Closed-Loop, Variable—Delay Stress Steering

This section describes stress steering that is performed continuously for each die and for each switching pulse. The dies that tend to be hotter are activated with a delay, the duration of which is decided by a closed-loop temperature controller. The delay can be in the range of microseconds for slow-switching devices with predominantly conduction losses or nanoseconds for fast switching devices with predominantly commutation losses.

The target losses of (13) can be described as a function of the unchangeable losses, P_{cte}, such the conduction, turn-OFF and some amount of the turn-ON losses, and the part of the turn-ON losses that is modified through the time delay $\overrightarrow{\delta t} = [\delta t_1, \ldots, \delta t_n]^T$. These losses P_{on} can be approximated by (14), for a delay smaller than the total rising time of the load current through the switch. The losses, P_{on}, modified by the delay correspond to the rising time of the switched current. Then, the commutation time and the total switched current are given in (15) and (16), respectively. Finally, (17) represents the loss distribution between the dies

$$\vec{P} = \overrightarrow{P_{cte}} + \overrightarrow{P_{\text{ON}}}\left(\overrightarrow{\delta t}\right) \tag{13}$$

$$\overrightarrow{P_{\text{ON}}}\left(\overrightarrow{\delta t}\right) = V_{\text{bus}} \cdot F_{\text{PWM}} \cdot I_{sw}\left(\overrightarrow{\delta t}\right) \cdot t_{sw}\left(\overrightarrow{\delta t}\right)/2 \tag{14}$$

$$t_{sw}\left(\overrightarrow{\delta t}\right) = \frac{I_{\text{Load}}}{N \cdot di/dt} + \frac{1}{N} \cdot [M] \times \overrightarrow{\delta t} \tag{15}$$

$$I_{sw}\left(\overrightarrow{\delta t}\right) = \frac{I_{\text{Load}}}{N} + \frac{di/dt}{N} \cdot [M] \times \overrightarrow{\delta t} \tag{16}$$

where

$$[M] = \begin{bmatrix} 1-N & 1 & \cdots & 1 \\ 1 & 1-N & \ddots & \vdots \\ \vdots & \ddots & \ddots & 1 \\ 1 & \cdots & 1 & 1-N \end{bmatrix}$$

with M being a N × N matrix

$$\overrightarrow{P_{\text{ON}}} = V_{\text{bus}} \cdot F_{\text{PWM}} \cdot \left(\frac{di}{dt} \cdot \frac{1}{N^2} \cdot \left([M] \times \overrightarrow{\delta t}\right)^2 + \frac{2I_{\text{Load}}}{N^2} \cdot [M] \times \overrightarrow{\delta t} + \frac{2I_{\text{Load}}^2}{N^2 di/dt}\right). \tag{17}$$

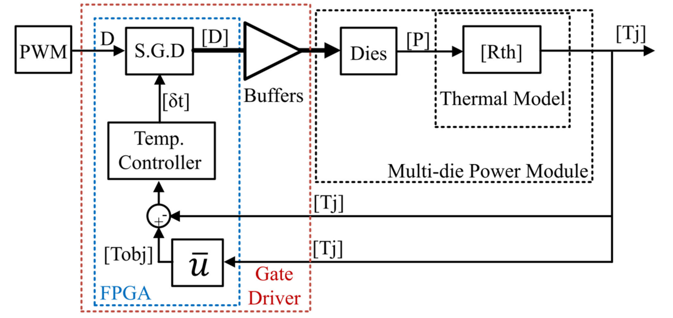

Fig. 18. Selective gate driving: reduction of peak junction temperatures with application of a driving profile for a power module with MG access compared to the reference SG power module.

The thermal regulation system is shown in Fig. 18 where the applied PWM is modified by the *Temp. Controller* to produce a specific power profile, $\vec{P}$, according to (13). The delay applied to the input PWM pattern for each die can be derived from the error between the average measured temperatures of all the dies, and the individual die temperature using the TSEP-based method. Using this error, a scheduling controller removes or adds delay to each die. The controller is a multivariable proportional integral compensator with the transfer function as per (18) and (19). Hence, the temperature can be balanced between all parallel dies online during the operation of the converter

$$\overrightarrow{\delta t} = \overrightarrow{\delta t'} - \min\left(\overrightarrow{\delta t'}\right) \tag{18}$$

$$\overrightarrow{\delta t'} = \begin{pmatrix} P + I \cdot s & 0 & \cdots & 0 \\ 0 & \ddots & \ddots & \vdots \\ \vdots & \ddots & \ddots & 0 \\ 0 & \cdots & 0 & P + I \cdot s \end{pmatrix} \cdot (T_j - \overline{T_j}) \tag{19}$$

where s is the Laplace variable.

As a demonstration, an air-cooled prototype power module was constructed from two parallel six-pack power modules, CM150TX-24S1 from Mitsubishi Electric, as shown in Fig. 19(a). Each switch thus comprises six dies, distributed in two different packages. The FPGA employed for prototype is a Xilinx Spartan-6 with a 100 MHz clock, paired with a 16-bit AD7626 Adc). This is incorporated in a back-to-back full bridge converter developed for a 500 V dc bus [see Fig. 19(b)]. The temperature has been measured using the TSEP-based method described in Section III-C and verified with an infrared camera.

Loading the prototype power module causes an unequal temperature distribution across the set of parallel dies, with a maximum difference of 23°C from the coldest to hottest die, as shown in Fig. 20(a) (open loop). This dispersion is attributed to the air cooling employed, inequality in thermal paths and die parameter dispersal. The maximum current handling capability of the power module is limited by the hottest die, in this case die 5. After enabling the temperature balancing control, the maximum temperature at the same loading condition decreases toward the mean temperature by 12°C, and the previously coldest die increases by nearly the same amount, as shown in Fig. 20(a) (closed loop). In this case, if the load current capability is fixed by

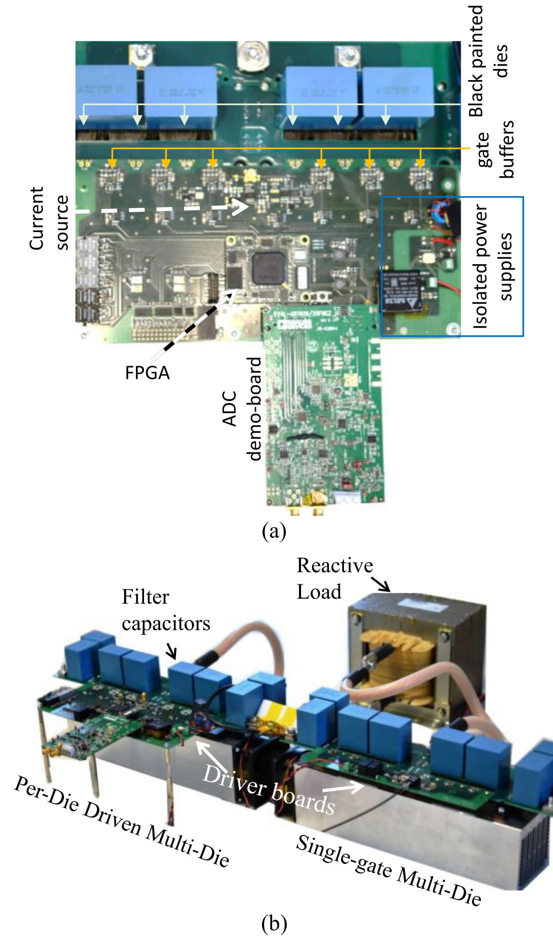

Fig. 19. Experimental IGBT prototype. (a) gate driver with junction temperature measurement as per Figs. 6 and 7. (b) Back to back configuration.

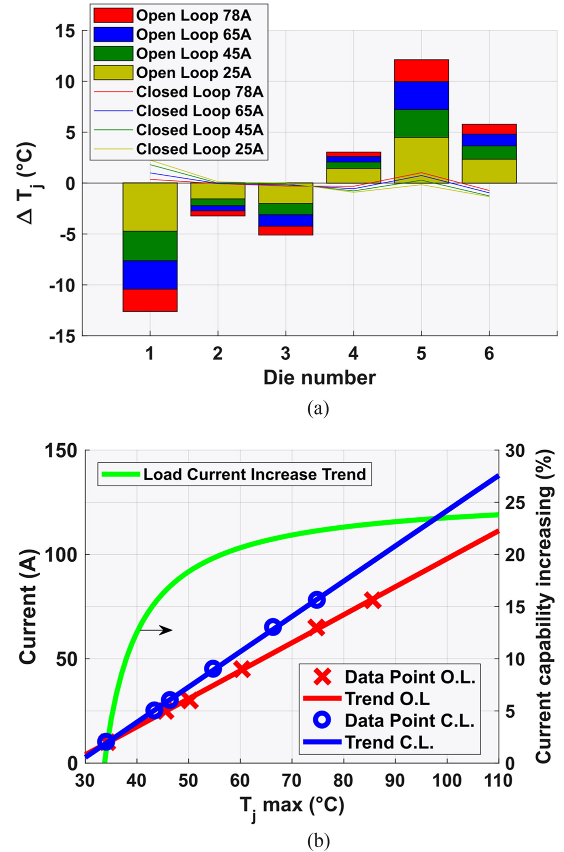

Fig. 20. Application of temperature balancing the prototype power module at 500V and 10 kHz. (a) Difference in temperature relative to the mean temperature with balanced and unbalanced temperatures. (b) Load current handling capability increase.

TABLE III
JUNCTION TEMPERATURES VDC = 500 V, PWM = 10 kHz, AND TAMB = 25 °C

Current (A)	Junction temperatures (°C)					
	Maximum			Average		
	O.L.	C.L.	Diff.	O.L.	C.L.	Diff.
10	34,2	34,1	-0,1	31,8	32,0	0,2
25	45,5	43,4	-2,0	41,0	41,2	0,2
30	50,2	46,4	-3,8	44,9	44,4	-0,5
45	60,3	54,8	-5,5	53,1	53,0	-0,1
65	74,6	66,4	-8,2	64,7	65,4	0,7
78	85,6	74,8	-10,7	73,5	73,9	0,4

the maximum junction temperature of any given die, the power module with more even thermal loading is capable of withstanding more losses. Therefore, the load current can be increased, and the power density of the power module can be improved. Importantly, the above experiment also demonstrates the method applied to a set of dies distributed in two separate packages, addressing also the problem of stress sharing between parallel power modules. Also, the closed-loop method will sustain this stress distribution throughout the lifecycle of the module.

In order to better visualize the effect of balancing the die temperatures on the load current handling capability of the power module, Fig. 20(b) illustrates the power module with no selective driving pattern applied (i.e., open loop with no temperature balancing) and closed-loop conditions (i.e. with temperature balancing for a given load current). As an example, on the 25 A point, the controller applies a delay equals to $\overrightarrow{\delta t} = [0,\ 140,\ 70,\ 140,\ 300,\ 160]$ns on the dies 1 to 6, respectively. As the load current increases, the difference between the maximum junction temperatures of the two solutions increases. Hence, for a fixed maximum junction temperature, there is an associated load current handling capability of the power module. In this experimental prototype, the selective gate drive method permits an increase of 25% in the current handling capability, assuming a maximum junction temperature of 150°C for the hottest die.

Table III shows the maximum and average temperatures for the operating points of Fig. 20. While the maximum temperature could be reduced for all operating points, the average temperature is maintained in a range of $+/-1$°C, the precision of the temperature measurement. This indicates that the efficiency of the multidie power module is unaffected by the applied stress-steering.

A demonstration video of the online thermal equalization is shown in [49]. The switch to thermal equalization mode, performed in real time, occurs at 1 min 31s in the video.

V. Conclusion

In this article, a method that implements selective gate driving for an intelligent power module is presented as a solution to accommodate the use of smaller, more numerous dies within a multidie power module. By incorporating individual gate driving, the switching losses can be reduced, and several condition monitoring features such individual junction temperature estimation and indirectly measuring the saturation voltage in the power module can be performed. Furthermore, by incorporating the individual junction temperature estimation and the selective gate driving technique, the individual dies within the power module can be better utilized, thereby enabling a substantial increase in the load current handling capability of the power module. The technique presented in this article is applicable to highly integrated large-current intelligent power modules based on wide bandgap semiconductors with inherently smaller, more numerous dies.

An interesting corollary to the proposed thermal equalization solution is that it enables unrestricted paralleling of small power modules to achieve a very large current rating which, together with the inherent condition monitoring features, would allow significant cost reductions for high power, mission-critical applications.

Finally, a switching power cycling tests bench has been running the proposed junction temperature algorithm consistently for over two years. The resulting lifetime extension and the use of the generated data for condition monitoring purposes will be discussed in a forthcoming article.

References

[1] H. Wang, M. Liserre, and F. Blaabjerg, "Toward reliable power electronics: Challenges, design tools, and opportunities," *IEEE Ind. Electron. Mag.*, vol. 7, no. 2, pp. 17–26, Jun. 2013.

[2] The Highly Efficient and Reliable smart Transformer (HEART), Jan. 2020. [Online]. Available. http://www.heart.tf.uni-kiel.de/en/home/

[3] Reliable Power Electronics (ReliPE), Jan. 2020. [Online]. Available. https://www.sintef.no/en/reliable-power-electronics/

[4] E. A. Jones, F. F. Wang, and D. Costinett, "Review of commercial GaN power devices and GaN-based converter design challenges," *IEEE J. Emerg. Sel. Top. Power Electron.*, vol. 4, no. 3, pp. 707–719, Sep. 2016.

[5] J. Roberts, J. Styles, and D. Chen, "Integrated gate drivers for e-mode very high power GaN transistors," in *Proc. IEEE Int. Workshop Integr. Power Packag*., 2015, pp. 16–19.

[6] M. Giandalia and D. Kinzer, "System integration benefits of GaN Power ICs," in *Proc. Eur. Int. Exhib. Conf. Power Electron., Intell. Motion, Renew. Energy Energy Manage.*, 2019, pp. 1–6.

[7] H. Li *et al.*, "Influence of paralleling dies and paralleling half-bridges on transient current distribution in multichip power modules," *IEEE Trans. Power Electron.*, vol. 33, no. 8, pp. 6483–6487, Aug. 2018.

[8] S. Weihua, L. Ran, Z. Zheng, L. Xiaoling, and P. Mawby, "Design and evaluation of SiC multichip power module with low and symmetrical inductance," *J. Eng.*, vol. 2019, no. 17, pp. 3573–3577, Jun. 2019.

[9] C. Chen, F. Luo, and Y. Kang, "A review of SiC power module packaging: Layout, material system and integration," *CPSS Trans. Power Electron. Appl.*, vol. 2, no. 3, pp. 170–186, Sep. 2017.

[10] J. Ewanchuk, J. Brandelero, and S. V. Mollov, "Improving the die utilization and lifetime in multi-die SiC power module by means of integrated per-die gate buffers," in *Proc. 29th Int. Symp. Power Semicond. Devices ICs*, 2017, pp. 439–442.

[11] J. Ewanchuk, J. Brandelero, and S. Mollov, "A gate driver based approach to improving the current density in a power module by equalizing the individual die temperatures," in *Proc. IEEE Energy Convers. Congr. Expo.*, 2018, pp. 4652–4658.

[12] S. Zhao *et al.*, "Adaptive multi-level active gate drivers for SiC power devices," *IEEE Trans. Power Electron.*, vol. 35, no. 2, pp. 1882–1898, Feb. 2020.

[13] Y. Yang, Y. Wen, and Y. Gao, "A novel active gate driver for improving switching performance of high-power SiC MOSFET modules," *IEEE Trans. Power Electron.*, vol. 34, no. 8, pp. 7775–7787, Aug. 2019.

[14] A. P. Camacho, V. Sala, H. Ghorbani, and J. L. R. Martinez, "A novel active gate driver for improving SiC MOSFET switching trajectory," *IEEE Trans. Ind. Electron.*, vol. 64, no. 11, pp. 9032–9042, Nov. 2017.

[15] G. Engelmann, T. Senoner, and R. W. De Doncker, "Experimental investigation on the transient switching behavior of SiC MOSFETs using a stage-wise gate driver," *CPSS Trans. Power Electron. Appl.*, vol. 3, no. 1, pp. 77–87, 2018.

[16] Y. Avenas, L. Dupont, N. Baker, H. Zara, and F. Barruel, "Condition monitoring: A decade of proposed techniques," *IEEE Ind. Electron. Mag.*, vol. 9, no. 4, pp. 22–36, Dec. 2015.

[17] U.-M. Choi, F. Blaabjerg, S. Jorgensen, S. Munk-Nielsen, and B. Rannestad, "Reliability improvement of power converters by means of condition monitoring of IGBT modules," *IEEE Trans. Power Electron.*, vol. 32, no. 10, pp. 7990–7997, Oct. 2017.

[18] H. Oh, B. Han, P. Mccluskey, C. Han, and B. D. Youn, "Physics-of-failure, condition monitoring, and prognostics of insulated gate bipolar transistor modules: A review," *IEEE Trans. Power Electron.*, vol. 30, no. 5, pp. 2413–2426, May 2015.

[19] M. A. Eleffendi and C. M. Johnson, "Application of kalman filter to estimate junction temperature in IGBT power modules," *IEEE Trans. Power Electron.*, vol. 31, no. 2, pp. 1576–1587, Feb. 2016.

[20] B. Ji *et al.*, "In situ diagnostics and prognostics of solder fatigue in IGBT modules for electric vehicle drives," *IEEE Trans. Power Electron.*, vol. 30, no. 3, pp. 1535–1543, Mar. 2015.

[21] T. A. Polom, C. van der Broeck, R. W. De Doncker, and R. D. Lorenz, "Real-time, in situ degradation monitoring in power semiconductor converters," in *Proc. IEEE Appl. Power Electron. Conf. Expo.*, 2019, pp. 2720–2727.

[22] X. Wang *et al.*, "Current sharing of IGBT modules in parallel with thermal imbalance," in *Proc. IEEE Energy Convers. Congr. Expo.*, 2010, pp. 2101–2108.

[23] N. Chen, F. Chimento, M. Nawaz, and L. Wang, "Dynamic characterization of parallel-connected high-power IGBT modules," *IEEE Trans. Power Electron.*, vol. 51, no. 1, pp. 539–546, Jan./Feb. 2015.

[24] H. Li *et al.*, "Influences of device and circuit mismatches on paralleling silicon carbide MOSFETs," *IEEE Trans. Power Electron.*, vol. 31, no. 1, pp. 621–634, Jan. 2016.

[25] P. Hofer, N. Karrer, and C. Gerster, "Paralleling intelligent IGBT power modules with active gate-controlled current balancing," in *Proc. PESC Rec. 27th Annu. IEEE Power Electron. Spec. Conf.*, 1996, vol. 2, pp. 1312–1316.

[26] S. Teuber, M. Honsberg, A. Kubitz and G. Katzenberger, "IGBT power stage delay calibration is minimizing current imbalance in large power modules with isolated multiply segmented paralleled half bridges," in *Proc. Eur.Int. Exhib. Conf. Power Electron., Intell. Motion, Renew. Energy Energy Manage.*, 2018, pp. 1–7.

[27] K. Matsubara and K. Wada, "Current balancing for parallel connection of silicon carbide MOSFETs using bus bar integrated magnetic material," in *Proc. IEEE Appl. Power Electron. Conf. Expo.*, 2019, pp. 2688–2693.

[28] J. Wang, Z. Li, X. Jiang, C. Zeng, and Z. J. Shen, "Gate control optimization of Si/SiC hybrid switch for junction temperature balance and power loss reduction," *IEEE Trans. Power Electron.*, vol. 34, no. 2, pp. 1744–1754, Feb. 2019.

[29] Z. Zeng, X. Zhang, and X. Li, "Layout-dominated dynamic current imbalance in multichip power module: mechanism modeling and comparative evaluation," *IEEE Trans. Power Electron.*, vol. 34, no. 11, pp. 11199–11214, Nov. 2019.

[30] B. Zhang and S. Wang, "Parasitic inductance modeling and reduction for a wire bonded half bridge SiC MOSFET multichip power module," in *Proc. IEEE Appl. Power Electron. Conf. Expo.*, 2019, pp. 656–663.

[31] S. Weihua, L. Ran, Z. Zheng, L. Xiaoling, and P. Mawby, "Design and evaluation of SiC multichip power module with low and symmetrical inductance," *J. Eng.*, vol. 2019, no. 17, pp. 3573–3577, 2019.

[32] H. Li *et al.*, "A novel DBC layout for current imbalance mitigation in SiC MOSFET multichip power modules," *IEEE Trans. Power Elect.*, vol. 31, no. 12, pp. 8042–8045, Dec. 2016.

[33] D. Reusch and J. Strydom, "Effectively paralleling gallium nitride transistors for high current and high frequency applications," in *Proc. IEEE Appl. Power Electron. Conf. Expo.*, 2015, pp. 745–751.

[34] Z. Zeng, X. Zhang, and X. Li, "Influence of kelvin connection on current dispatching in multichip power module: mechanism modeling and comparative evaluation," *IEEE Trans. Power Electron.*, vol. 34, no. 11, pp. 11199–11214, Nov. 2019.

[35] Y. Xiao, H. Shah, T. P. Chow, and R. J. Gutmann, "Analytical modeling and experimental evaluation of interconnect parasitic inductance on MOSFET switching characteristics," in *Proc. IEEE Appl. Power Electron. Conf. Expo.* , 2004, vol. 1, pp. 516–521.

[36] N. Chen, F. Chimento, M. Nawaz, and L. Wang, "Dynamic characterization of parallel-connected high-power IGBT modules," *IEEE Trans. Ind. Appl.*, vol. 51, no. 1, pp. 539–546, Jan./ Feb. 2015.

[37] M. Denk and M. Bakran, "Comparison of U CE - and R Gi -based junction temperature measurement of multichip IGBT power modules keywords 1 introduction 2 measurement methods and test setup," in *Proc. 17th Eur. Conf. Power Electron. Appl.*, 2015, pp. 1–11.

[38] N. Baker, L. Dupont, S. Munk-Nielsen, F. Iannuzzo, and M. Liserre, "IR camera validation of IGBT junction temperature measurement via peak gate current," *IEEE Trans. Power Electron.*, vol. 32, no. 4, pp. 3099–3111, Apr. 2017.

[39] N. Baker, S. Munk-Nielsen, F. Iannuzzo, and M. Liserre, "IGBT junction temperature measurement via peak gate current," *IEEE Trans. Power Electron.*, vol. 31, no. 5, pp. 3784–3793, May 2016.

[40] M. Denk and M. Bakran, "Junction temperature measurement during inverter operation using a TJ-IGBT-Driver," in *Proc. Eur. Int. Exhib. Conf. Power Electron., Intell. Motion, Renew. Energy Energy Manage.*, 2015, pp. 1–8.

[41] J. Brandelero, J. Ewanchuk, and S. Mollov, "On-line virtual junction temperature measurement via DC gate current injection," in *Proc. 10th Int. Conf. Integr. Power Electron. Syst.*, 2018, pp. 1–7.

[42] N. Baker and F. Iannuzzo, "The temperature dependence of the flatband voltage in high-power IGBTs," *IEEE Trans. Ind. Electron.*, vol. 66, no. 7, pp. 5581–5584, Jul. 2019.

[43] J. Brandelero, L.M. Alonso, J. Ewanchuk, and S. V. Mollov, "Indirect on-state voltage estimation using a voltage sensitive electrical parameter through the gate driver," in *Proc. PCIM Eur. Int. Exhib. Conf. Power Electron., Intell. Motion, Renew. Energy Energy Manage.*, 2019, pp. 5581–5584.

[44] D. Bortis, P. Steiner, J. Biela, and J. W. Kolar, "Double-stage gate drive circuit for parallel connected IGBT modules," *IEEE Trans. Dielect. Elect. Insul.*, vol. 16, no. 4, pp. 1020–1027, Aug. 2009.

[45] Y. Lobsiger, D. Bortis and J. W. Kolar, "Decentralized active gate control for current balancing of parallel connected IGBT modules," in *Proc. 14th Eur. Conf. Power Electron. Appl.*, 2011, pp. 1–10.

[46] Y. Chen, F. Zhuo, W. Pan, F. Zhang, and L. Feng, "A novel active gate driver for static and dynamic current balancing of parallel-connected IGBTs," in *Proc. IEEE Appl. Power Electron.*, 2017, pp. 795–799.

[47] J. Ewanchuk, J. Brandelero, and S. Mollov, "Lifetime extension of a multi-die SiC power module using selective gate driving with temperature feedforward compensation," in *Proc. IEEE Energy Convers. Congr. Expo.*, 2017, pp. 2520–2526.

[48] J. Lu, R. Hou, and D. Chen, "Loss distribution among paralleled GaN HEMTs," in *Proc. IEEE Energy Convers. Congr. Expo*., 2018, pp. 1914–1919.

[49] Thermal equalization Video, 2020. [Online]. Available: https://youtu.be/hPBHLPJ7KXU

Julio Brandelero (Member, IEEE) received the B.S. degree from the Federal University of Santa Catarina, Florianópolis, Brazil, the B.S and M.S degrees from the INPT—ENSEEIHT, Toulouse, France, and the Ph.D. degree from the National Polytechnic Institute of Toulouse, Toulouse, France, with the Laplace Laboratory and Cirtem, in 2015.

In 2015, he joined the Power Electronic Systems Division with the Mitsubishi Electric R&D Centre Europe in Rennes, where he conducts research related to condition monitoring, reliability and robustness of power converters. His research activity focused on power electronics application in the field of the more electrical aircraft.

Jeffrey Ewanchuk (Member, IEEE) received the B.Sc. degree (with distinction) in electrical engineering, the M.Sc. degree in power electronics, and the Ph.D. degree in energy systems from the University of Alberta, Edmonton. AB, Canada, in 2006, 2008 and 2012, respectively.

From 2008 to 2009, he was a Design Engineer with RMS Welding Systems, Nisku, AB, Canada. In 2012, he joined Mitsubishi Electric Research Centre Europe in Rennes, France, as a Research Engineer in power electronics, afterward taking position as a Senior Staff Research Engineer, and then later as a Research Manager. Since 2019, he has been a Staff Engineer in power electronics packaging with the Research Center, Raytheon Technologies, East Hartford, CT, USA. His current research interests include highly integrated power converters, high density packaging concepts, and the design consequences on the power converter lifetime and robustness.

Stefan Mollov (Member, IEEE) received the Dipl. Eng. degree from the Technical University of Gabrovo, Gabrovo, Bulgaria, in 1995, and the Ph.D. degree from the University of Birmingham, Birmingham, U.K., in 1998.

From 2000, he was a Lecturer with the University of Birmingham, where his research activities focused on power electronics applications in the field of autonomous systems, aerospace electrical systems, and renewable energy sources and storage. In 2005, he joined ADETEL Group, France, as a Power Electronics Expert, working on transportation applications. In 2009, he joined THALES Avionics, as a Power Supply Expert. Since 2013, he has been the Head of the Power Electronic Systems Division, Mitsubishi Electric R&D Centre Europe, Rennes, France, with activities covering reliability, diagnostics and prognostics and optimal design of highly integrated power conversion equipment.